iScience

CellPress
OPEN ACCESS

Article

Proteolysis and multimerization regulate signaling along the two-component regulatory system AdeRS

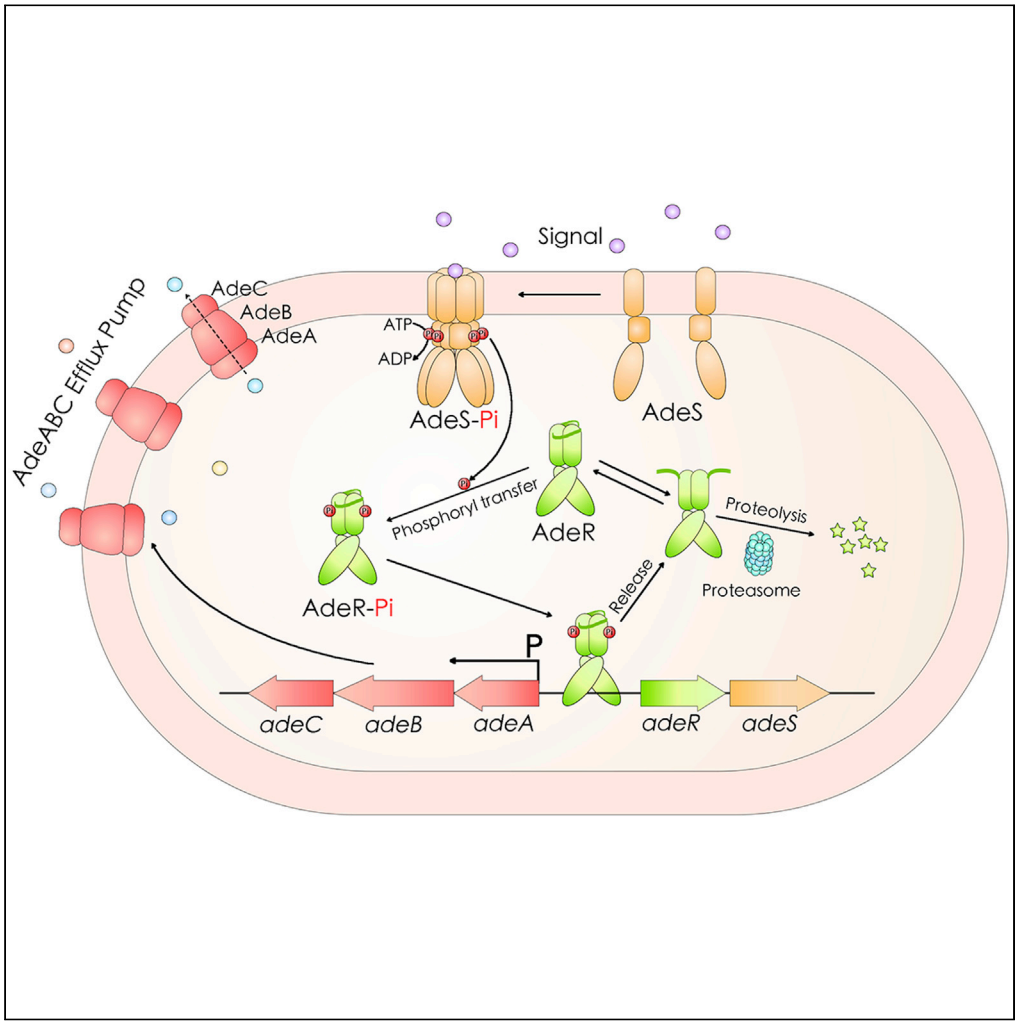

Zhenlin Ouyang, Fang Zheng, Li Zhu, ..., Peter M. Hwang, Junjun She, Yurong Wen

sjuns@sina.com (J.S.)
yurong.wen@xjtu.edu.cn (Y.W.)

Highlights

Crystal structure of AdeR dimer with traceable N-terminal intrinsically disordered region.

N-terminal intrinsically disordered region AdeR is involved in proteasome proteolysis.

Crystal structure of AdeS catalytic domain demonstrates *cis* autophosphorylation.

AdeS can assemble into hexamer and is crucial for its full kinase activity.

Ouyang et al., iScience 24, 102476
May 21, 2021
https://doi.org/10.1016/j.isci.2021.102476

iScience

CellPress
OPEN ACCESS

Article

Proteolysis and multimerization regulate signaling along the two-component regulatory system AdeRS

Zhenlin Ouyang,[1,6] Fang Zheng,[2,6] Li Zhu,[3,6] Jan Felix,[4] Di Wu,[3] Ke Wu,[3] Irina Gutsche,[4] Yi Wu,[2] Peter M. Hwang,[5] Junjun She,[1,*] and Yurong Wen[1,2,7,*]

SUMMARY

Bacterial two-component regulatory systems are ubiquitous environment-sensing signal transducers involved in pathogenesis and antibiotic resistance. The *Acinetobacter baumannii* two-component regulatory system AdeRS is made up of a sensor histidine kinase AdeS and a cognate response regulator AdeR, which together reduce repression of the multidrug-resistant efflux pump AdeABC. Herein we demonstrate that an N-terminal intrinsically disordered tail in AdeR is important for the upregulation of *adeABC* expression, although it greatly increases the susceptibility of AdeR to proteasome-mediated degradation. We also show that AdeS assembles into a hexameric state that is necessary for its full histidine kinase activity, which appears to occur via *cis* autophosphorylation. Taken together, this study demonstrates new structural mechanisms through which two-component systems can transduce environmental signals to impact gene expression and enlightens new potential antimicrobial approach by targeting two-component regulatory systems.

INTRODUCTION

Two-component regulatory systems (TCSs) are ubiquitous phosphorelay signal transduction proteins, critical for sensing and responding to environmental stimuli (Groisman, 2016; Stock et al., 2000). As the TCSs are abundant in bacterial genomes and respond to a wide variety of stimuli including temperature, pH, osmotic pressure, metabolic substrates, and many other signals, they are therefore important in host-pathogen interactions, bacterial pathogenesis, and antibiotic resistance. The TCSs also represent potential antimicrobial drug targets, both for broad-spectrum and precisely targeted therapy (Gotoh et al., 2010).

Acinetobacter baumannii ranks as the top critical threat among the multidrug-resistant bacteria according to the World Health Organization, possessing an extraordinary capacity for developing multidrug resistance. The *adeRS-adeABC* cluster has been extensively reported to mediate multidrug resistance against many antibiotics, including aminoglycosides, fluoroquinolones, tigecycline, and chloramphenicol (Marchand et al., 2004; Yoon et al, 2013, 2015). The *A. baumannii* TCS AdeRS directly reduces repression of the efflux pump AdeABC by binding to an intercistronic region between *adeRS* and *adeABC* (Wen et al., 2017). A diversity of mutations in both the histidine kinase AdeS and response regulator AdeR strongly associates these proteins with antimicrobial resistance in *A. baumannii* (Gerson et al., 2018; Nowak et al., 2016; Yoon et al., 2013).

In the canonical TCS, the transmembrane sensor histidine kinase undergoes a conformational change upon sensing an external environment stimulus and auto-phosphorylates at a conserved histidine residue using ATP. The phosphate group can then be transferred to an aspartate residue in the cognate response regulator, which then initiates a response by modulating target gene expression (Capra and Laub, 2012; Groisman, 2016; Stock et al., 2000). Owing to the tremendous numbers of TCSs and the diverse environmental stimuli to which they respond, there have been multiple modes of activation reported both in sensor histidine kinases and response regulators (Desai and Kenney, 2017; Willett and Crosson, 2017).

In this study, we characterize how conformational changes are propagated along the *A. baumannii* AdeRS TCS. We have found a new mechanism whereby the activity of the response regulator AdeR is dependent upon the presence of an intrinsically disordered N-terminal tail. We also determine the structure of the histidine kinase transmitter domain of AdeS using X-ray crystallography and demonstrate, via negative stain

[1]Talent Highland and Center for Gut Microbiome Research of Med-X Institute, The First Affiliated Hospital, Xi'an Jiaotong University, Xi'an 710061, China

[2]The Key Laboratory of Environment and Genes Related to Disease of Ministry of Education, Health Science Center, Xi'an Jiaotong University, Xi'an 710061, China

[3]MOE Key Laboratory of Cell Activities and Stress Adaptations, School of Life Sciences, Lanzhou University, Lanzhou, China

[4]Institut de Biologie Structurale, Univ. Grenoble Alpes, CEA, CNRS, IBS, 71 avenue des Martyrs, Grenoble F-38044, France

[5]Departments of Medicine and Biochemistry, Faculty of Medicine & Dentistry, University of Alberta, Edmonton, Alberta T6G 2R3, Canada

[6]These authors contributed equally

[7]Lead contact

*Correspondence: sjuns@sina.com (J.S.), yurong.wen@xjtu.edu.cn (Y.W.)

https://doi.org/10.1016/j.isci.2021.102476

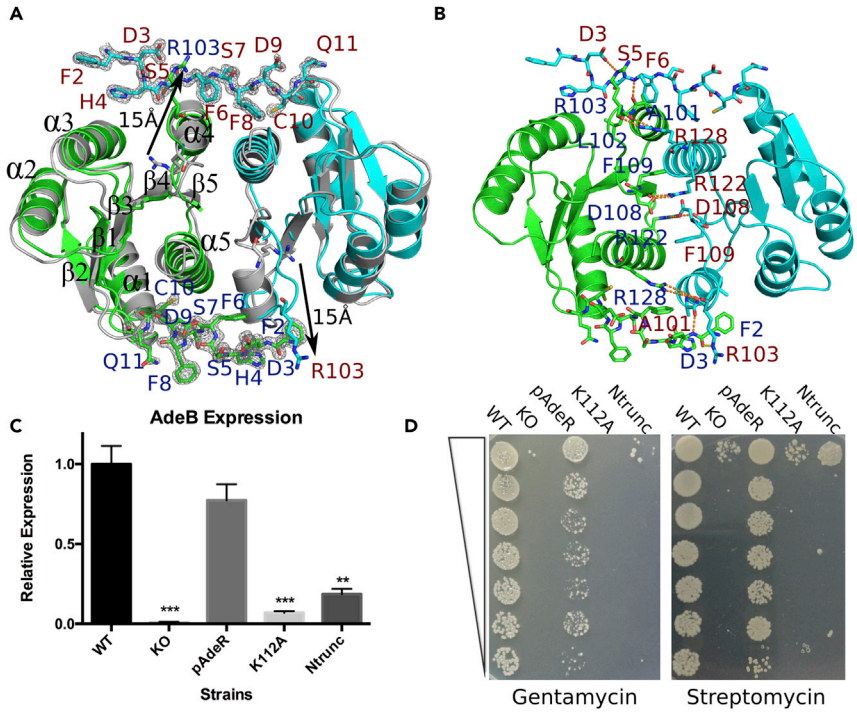

Figure 1. Structural alignment of response regulator AdeR wild-type versus K112A mutant with ordered N-terminal tail

(A) The dimer of K112A-AdeR with visible N terminus is colored with green and cyan, and the dimer of wild-type AdeR is colored in gray. The N-terminal tail residues 2–11 are shown in stick format with density contours at 3σ.

(B) Detailed interaction between the dimer interface of AdeR with N terminus.

(C) RT-qPCR detection of *adeB* levels in different AdeR constructs. Truncation of the AdeR N terminus decreases the expression of the efflux pump component AdeB.

(D) Antimicrobial susceptibility testing through agar dilution of wild-type, AdeR knockout, pBAD-AdeR, and N-terminal truncation mutant demonstrates that the N-terminal domain is crucial for its antimicrobial resistance.

electron microscopy and small-angle X-ray scattering (SAXS), that the full cytoplasmic domain of AdeS forms a hexamer in solution necessary for its histidine kinase activity. The present investigation sheds light on new structural mechanisms whereby signals are transduced and regulated along the TCS AdeRS in *A. baumannii*.

RESULTS

AdeR possesses an N-terminal intrinsically disordered region that is essential for its regulation

Structure-based sequence alignment of *A. baumannii* response regulator AdeR with other response regulator family indicates that it contains an extended N-terminal sequence, "FDHSFSFDCQD," which consists of three hydrophobic F and three acidic D residues (Figure S1). The electron density of this tail could not be observed in the 1.4 Å resolution crystal structure of the AdeR receiver domain (Wen et al., 2017), indicating that it is disordered and able to adopt multiple conformations. Its disordered nature was further validated by SAXS (Wen et al., 2017). In the current study, crystallization and structure determination of an AdeR K112A mutant interestingly demonstrate a completely traceable N-terminal chain at 1.8 Å, running along a groove across the dimer interface formed by helices α4 and α5 (Figures 1A and S2A, Table S1).

The binding of the ordered N-terminal region to the other AdeR monomer coincides with a rearrangement of the α4-β5-α5 dimerization interface, characterized by a 15 Å shift of residue R103 in the α4 helix, as indicated by an alignment of the structures of $AdeR_{WT}$ and $AdeR_{K112A}$ (Figure 1A) and a coloring of this alignment by root-mean-square deviation (Figure S2B). Between the two AdeR monomers in the crystal asymmetric unit, the exact conformation of the N-terminal tail varies, which is a further indication of its structural plasticity. However, a common feature in both observed conformations is the electrostatic interaction of the side chains of F6 and R128 with

the C-terminal end of helix α4 across the dimer interface. The structure reveals a multitude of dipoles with their negative ends oriented toward F6 and R128, including the non-hydrogen-bonded carbonyl oxygens of V99, M100, and A101 at the C-terminal end of helix α4, as well as the carbonyl oxygens of L102 and R103 (Figures 1B and S2A). These interactions re-orient and stabilize helix α4, lengthening it relative to the wild-type structure so that its N-terminal end extends further back to D93. In the crystal structure of wild-type AdeR, this arrangement is prevented by a steric clash between the β4-α4 loop and the side chain of K112, which is held in place by a salt bridge with D63. Hence, it appears that the K112A mutation is coupled to a re-orientation and increased structuring of both the α4 helix and the disordered N-terminal tail. These structural changes further lead to a rearrangement of the α4-β5-α5 dimerization interface, causing a small shift in the relative orientation of the monomers within the homodimer (Figures 1A and S2B).

To verify whether the intrinsically disordered N-terminal region is involved in the regulation of the efflux pump AdeABC, we tested transcription of the *adeB* gene and antimicrobial susceptibility upon truncation of the AdeR N-terminal intrinsically disordered region. Quantitative RT-PCR showed that truncation of the N-terminal tail results in decreased adeB expression (Figure 1C) and an increase in susceptibility to gentamicin and streptomycin (Figure 1D, Table S2). This suggests that the N-terminal tail is needed to fully activate *adeB* expression. The K112A mutation also decreased *adeB* expression and increased antibiotic susceptibility. The explanation for this result is that the K112 side chain hydrogen bonds to the phosphate group of phosphoaspartate in homologous response regulator proteins like PhoP. We thus propose that the observed structure of the K112A mutant of AdeR represents a conformation that is partially activated by disruption of the K112-D63 hydrogen bond and structuring of the N-terminal disordered tail, but full activation requires phosphorylation of D63 and its subsequent interaction with K112.

The N-terminal intrinsically disordered region of AdeR increases its susceptibility to proteolysis *in vivo*

The N terminus is extensively reported to be an important determinant of protein half-life *in vivo* via the N-end rule, which highlights the preference of the proteasome for certain N-terminal degradation signals (N-degrons) (Bachmair et al., 1986; Kim et al., 2014; Varshavsky, 2011). An N-terminal D, E, F, H, Q, or Y residue confers a short half-life to a protein, being readily recognized by the proteasome (Bachmair et al., 1986; Kim et al., 2014; Varshavsky, 2011). The intrinsically disordered N-terminal region of AdeR "FDHSFSFDCQD" has shown high frequency of D, F, H, and Q residues, so proteolytic processing would produce a new N-terminal tail that would be highly susceptible to proteasomal degradation.

We performed an *in vivo* proteolysis assay of AdeR with and without the intrinsically disordered N-terminal region in *A. baumannii*. Owing to the lack of a commercially available anti-AdeR antibody, we used an anti-His tag antibody to detect the C-terminal His-tagged AdeR expressed from our plasmid. The proteolysis assay demonstrates that AdeR is degraded *in vivo* with a half-life around 70 min, whereas truncation of the N-terminal region significantly slowed the rate of degradation (Figures 2A and 2B). Lactacystin and its derivative β-lactone are covalent inhibitors of the prokaryotic proteasome (Craiu et al., 1997; Ōmura and Crump, 2019), and addition of the β-lactone reduced the proteolysis rate of AdeR *in vivo* (Figures 2A and 2B). Thus, although the intrinsically disordered N-terminal region of AdeR is needed for maximal activation, its presence also renders it susceptible to proteasomal degradation.

We further tested whether truncation of the disordered N-terminal region of AdeR would modify its DNA-binding activity. Isothermal titration calorimetery demonstrated that N-terminally truncated AdeR interacts with its target DNA with similar binding affinity (Kd = 20 nM) and thermodynamic properties (Figure 2C) (Wen et al., 2017). Thus, although the N-terminal tail of AdeR is required for its maximal activation, it is not needed for high-affinity DNA binding. Instead, it could be acting through any of the following potential mechanisms: stabilization of an AdeR dimer configuration that distorts and activates bound DNA, recruitment of an unknown factor to the AdeR-DNA complex, or facilitation of AdeS-mediated phosphorylation of AdeR.

The HAMP domain of AdeS is essential for its assembly and kinase activity

The sensor histidine kinase AdeS consists of two transmembrane N-terminal helices linked by a short extracellular sensor domain (residue 34–61), a HAMP domain (residue 84–138), a DHp (dimerization histidine phosphotransfer) domain (residue 146–204), and a C-terminal catalytic ATP (CA)-binding domain

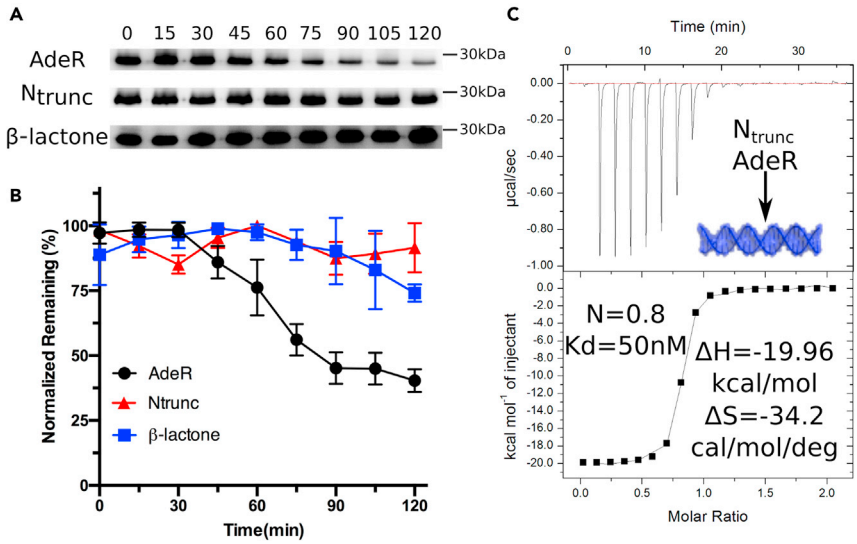

Figure 2. The effect of N-terminal truncation and supplement of proteasome inhibitor β-lactone on proteolytic degradation of AdeR

(A) Western blot of His-tag-detected recombinant AdeR (see STAR Methods section for details).

(B) Plot of band intensity versus time. The half-life of AdeR *in vivo* is around 60–80min, and the proteolysis of the AdeR can be attenuated by truncation of the intrinsically disordered N-terminal tail or by addition of the proteasome inhibitor β-lactone. Each time point is averaged from at least three independent experiments.

(C) Isothermal titration calorimetry of N terminus-truncated AdeR dimer with its recognition DNA sequence.

(residue 204–357) (Figure 3A). To investigate the kinetic properties of AdeS, we purified different recombinant constructs consisting of the AdeS full cytoplasmic domain (HAMP-DHp-CA), HAMP-DHp domain, and histidine kinase transmitter domain (DHp-CA), confirmed by SDS-PAGE (Figure 3B). The size exclusion chromatography profile indicated that the AdeS DHp-CA domain elutes as dimer with a calculated molecular weight of 47 kDa, whereas the cytoplasmic domain elutes with a calculated molecular weight around 190 kDa (Figure 3B), suggestive of a hexameric assembly. The HAMP-DHp domain elutes as a broader peak, which may imply a non-globular shape or the presence of mixed oligomers (Figure 3B).

RT-qPCR experiments of *adeB* expression indicated that the AdeS constructs lacking the transmembrane sensor domain still retain kinase activity *in vivo*. However, truncation of the HAMP domain or mutation of the catalytic histidine H149 totally abolishes its activity (Figure 3C). RT-qPCR detection of *adeB* expression also correlated with antibiotic minimum inhibitory concentration values determined for different AdeS construct strains (Table S3).

We further measured the kinase activity of the AdeS cytoplasmic domain and the DHp-CA domain (Figures 3D and 3E). The cytoplasmic domain has a Km of 5.25 $\pm$ 0.20 μM for ATP and Vmax of 1.1 μmol/mg•min^{-1} for autophosphorylation, whereas the DHp-CA domain alone displays no phosphoryl transfer activity (Figures 3D and 3E).

Crystal structure of AdeS DHp-CA domain and EM assembly of AdeS cytoplasmic domain

To further elucidate the molecular mechanism and assembly of AdeS, we carried out a combined X-ray crystallography and electron microscopy study of recombinant AdeS. The crystal structure of apo AdeS DHp-CA was solved by molecular replacement using a trimmed version of the catalytic domain of histidine kinase CpxA (PDB ID; 5FLK) (Mechaly et al., 2017), which has an overall sequence identity of 25% with AdeS (Figure S3), and an I-TASSER model of the DHp domain of AdeS as search templates. The AdeS DHp-CA domain consists of a symmetric homodimer, in which the α1-α2 DHp domain forms a central four helix bundle with a large parallel dimerization interface, which is flanked by CA domains on each side (Figure 4A). The conserved phosphorylation site histidine 149 is located at the N-terminal end of the α1 helix, whereas residues 138–147 were present in our DHp-CA construct but not visible in the crystal structure. This contrasts with CpxA, in which the α1 helix extends further N-terminally and is continuous with

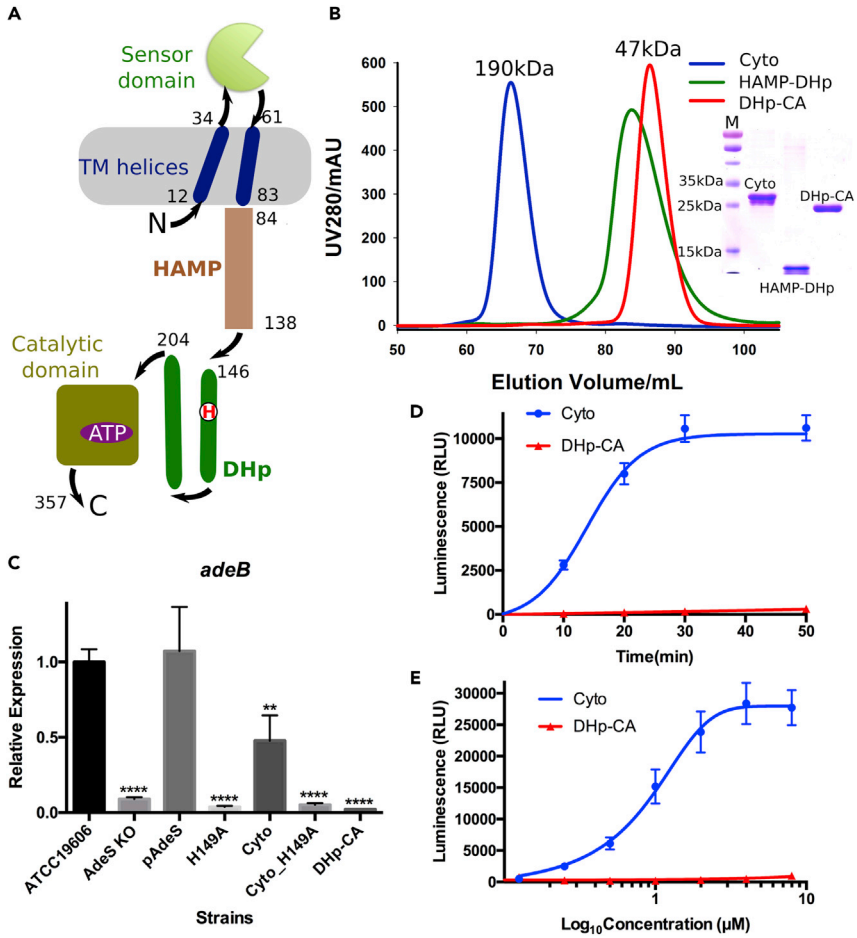

Figure 3. Characterization of histidine kinase AdeS

(A) Schematic view of histidine kinase AdeS domain organization.

(B) Size exclusion chromatography purification of AdeS cytoplasmic domain, HAMP-DHp domain, and DHp-CA domain.

(C) RT-qPCR experiments detecting *adeB* levels in *Acinetobacter baumannii* cells expressing different AdeS constructs. Note that the HAMP is essential for the AdeS activity.

(D and E) Kinetic assays of ATP hydrolysis by histidine kinase AdeS cytoplasmic domain and DHp-CA domain using luminescent detection of ADP in a concentration- (10 μM ATP for D) and time-dependent (30min for E) plotting. The cytoplasmic domain showed a Km of 5.25 ± 0.20 μM and Vmax of 1.1 μmol/mg•min^{-1} for autophosphorylation, whereas the DHp-CA domain alone showed no phosphoryl transfer activity.

the HAMP C-terminal helix (Figure S3). The α1 helix of AdeS extends from H149 to D167, followed by a short linker from G168-D173, leading to a long α2 helix from E174 to N202. The short interhelical linker in AdeS travels in a different direction and is longer than the corresponding linker in CpxA, so that the α2 helices are "swapped" when the homodimer of AdeS is compared with CpxA. This is why the CA domain in AdeS appears positioned to catalyze a *cis* autophosphorylation of His149 (within the same monomer), whereas CpxA appears to catalyze a trans-phosphorylation (Figure 4B).

A flexible linker between Q203 and N208 imparts a high degree of mobility to the CA domains when the structure of AdeS is compared with CpxA and other histidine kinases. In our AdeS structure, there are some hydrophobic contacts between the α1 helix (L197 and V200) of the DHp domain and the CA domain (V326 and A329), fixing the positioning of the CA domains. These must be transient for the CA domain to be able to move into the correct position to autophosphorylate H149 (Figures 4A and 4B). All the residues involved in the ATP binding and autophosphorylation are identical in AdeS and CpxA (Figure S3). Co-crystallization attempts for the AdeS full cytoplasmic domain and for DHp-CA domain with ATP, ADP, and ATP analogues were unsuccessful.

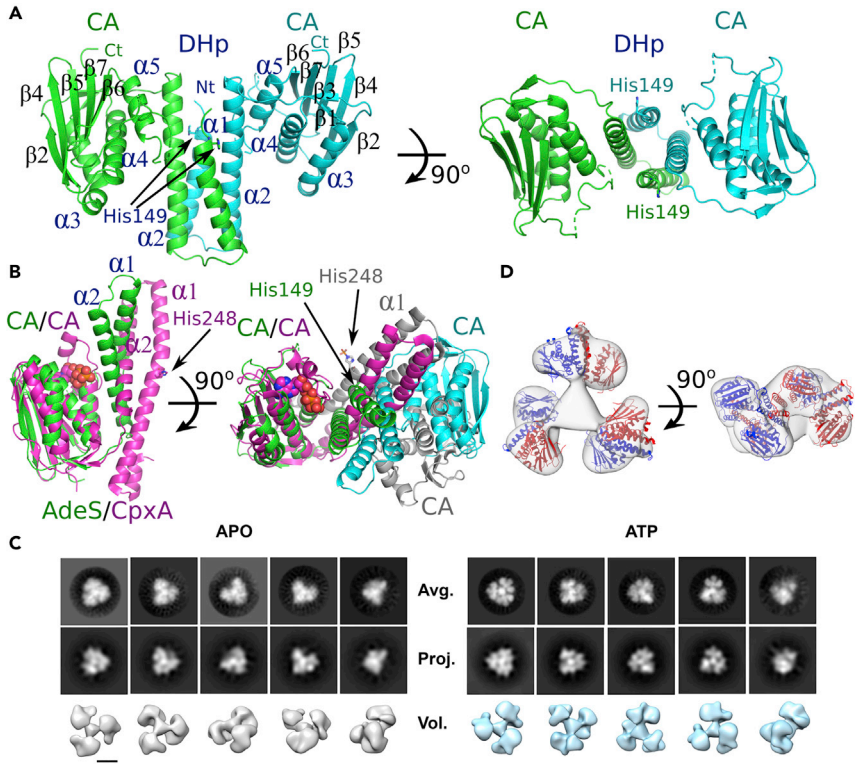

Figure 4. Crystal structure of histidine kinase AdeS DHp-CA domain and electron microscopy of histidine kinase AdeS full cytoplasmic domain (HAMP-DHp-CA)

(A) Overall structure of the AdeS DHp-CA domain, which adopts a canonical histidine kinase assembly and dimerizes through the DHp helix bundle. The His149 phosphorylation site is shown in stick.

(B) The alignment of AdeS (green) and CpxA (magenta) complexed with ATP with the CA domain superpositioned; the left panel and the right panel show monomer and the dimer views, ATP is shown in sphere and the conserved phosphorylation histidine is shown in stick. This indicated that the AdeS employs a *cis* autophosphorylation instead of *trans* autophosphorylation in CpxA.

(C) Reconstructions of histidine kinase in APO and ATP-bound states. Comparison between experimental 2D class average maps (top row) and corresponding projections (middle row) of cytoplasmic AdeS. The box size is 30.6 nm. The 3D reconstructions (surface mode, light gray in APO state and light sky blue in ATP-bound state) representing those related projections are shown at the bottom, with a scale bar of 5 nm added to the lower right corner of the first 3D model in APO state.

(D) The crystal structures of the DHp-CA domains (colored in red and blue cartoon) were docked into the EM structure of APO state (surface mode, light gray).

We therefore turned to direct visualization of the full cytoplasmic domain with negative stain electron microscopy, using a highly monodisperse preparation of purified cytoplasmic AdeS (HAMP-DHp-CA), both in the apo state and in the presence of ATP and Mg^{2+} (Figures 4C and S4). In total 619 and 319 micrographs were collected for the apo and ATP-bound states, respectively. After contrast transfer function estimation, 566 and 299 micrographs were screened out for the particle-picking procedure. About 37,000 particles for each individual dataset were used to do the 2D classification. Comparing the two class averages, more compact density distribution within each blade was observed in the ATP-bound state (Figure 4C). The gold-standard Fourier shell correlation curves at 0.143 criterion indicate a final resolution of 25 Å (apo state) and 22 Å (ATP-bound state), respectively (Figure S4). The projections obtained from certain Euler angles of the final model matched well with the experimental 2D class averages, with the three-blade propeller-like orientation corresponding to the top view of the 3D model (Figure 4C). We then manually docked our crystal structure of DHp-CA dimer into the two electron microscopic (EM) models by using the Fit-in-map routine of UCSF Chimera software. The crystal structures occupied the three blade-like densities outside well with the central joint-density vacant. It demonstrates that the DHp-CA dimers assemble further into a trimer-of-dimers mediated by the centrally located N-terminal HAMP domain. The arrangement requires greater flexibility between the HAMP domains and DHp domains than was observed in

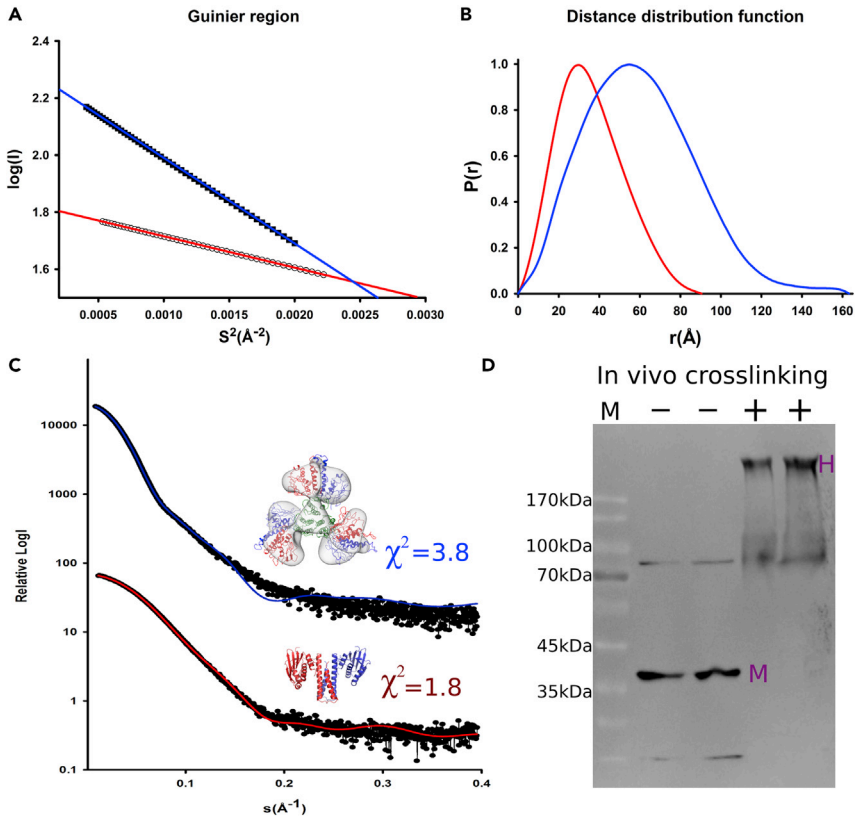

Figure 5. Solution and *in vivo* assembly of histidine kinase AdeS

(A and B) (A) Guinier region analysis and (B) distance distribution function analysis of AdeS DHp-CA (red) and cytoplasmic domain (blue) from small-angle X-ray scattering experiments.

(C) The fits of small-angle X-ray scattering experiment data with the AdeS DHp-CA dimer crystal structure model and the AdeS cytoplasmic hexameric model demonstrate high correlation with χ^2 values of 1.8 and 3.8, respectively.

(D) Formaldehyde cross-linking of full-length AdeS expressed in *Acinetobacter baumannii* ATCC19606 indicates that full-length AdeS forms an oligomeric/hexameric state *in vivo*. The +/− represents supplement of formaldehyde or not and the M/H indicate monomer/hexamer.

CpxA, and this may have contributed to the difficulty in crystallizing the full-length cytoplasmic AdeS construct. Comparison of the coordinates of the docked crystal structures shows a slightly clockwise rotation of the CA domains in the ATP-bound model relative to the apo model. Taken together, negative stain EM maps of the apo and ATP-incubated cytoplasmic AdeS both revealed an assembly into a hexamer, although the ATP-incubated cytoplasmic AdeS displayed better-defined CA domains, suggesting that there was a greater conformational heterogeneity in the apo state, with binding of ATP stabilizing a more uniform activated state (Figures 4D and S4).

Solution assembly and in cell cross-linking of AdeS

To further explore the physiological assembly of AdeS, we carried out SAXS and an in-cell cross-linking study. Plots of the Guinier region provide evidence of the overall high quality of the SAXS data, and corresponding distance distributions indicated the overall size of the measured samples (Figures 5A and 5B).

The SAXS data confirm the dimeric assembly of the AdeS DHp-CA domain and the hexameric assembly of the AdeS full cytoplasmic domain, as judged by the molecular weight calculated by MoW2 and the Porod volume approach, which is consistent with our results with size exclusion chromatography (Table S4). The AdeS DHp-CA domain SAXS experimental data strongly confirm its dimeric crystal structure with a X^2 value of 1.8. Furthermore, the AdeS full cytoplasmic domain model was generated by fitting three copies of the AdeS DHp-CA dimer and a hexameric HAMP domain model generated from I-TASSER in the negative stain EM map. The validation of the AdeS full cytoplasmic domain model with the SAXS experimental data using AllosMod-FoXS shows good agreement with the hexameric assembly in solution (Figure 5C) (Yang and Zhang, 2015).

To further verify the oligomeric state of full-length AdeS *in vivo*, we carried out an in-cell formaldehyde cross-linking experiment employing a low-copy-number full-length AdeS expression plasmid with His-tag. *A. baumannii* cells treated with and without formaldehyde were disrupted; the AdeS full-length protein was purified and detected by western blotting using an anti-His-tag antibody (Figure 5D). The results indicated that cross-linked AdeS behaved as an oligomer with a molecular weight higher than 170 kDa, whereas the sample without cross-linking behaved as a monomer on SDS-PAGE. Both samples showed a light band corresponding to a dimer population, which could have resulted from incomplete denaturation in SDS (Figure 5D). Taken together, our combined X-ray crystallographic/SAXS/negative stain EM study determines the physiological assembly of AdeS to be a trimer-of-dimers and allows us to propose a structural model for the full cytoplasmic domain of AdeS.

DISCUSSION

The mechanism by which signals are transduced along the ubiquitous TCSs remains a profound mystery because of a continuous chain of conformational transitions that must occur within each component. Perhaps the most easily understood part of the signal transduction is the transfer of a phosphate group from the histidine kinase sensor to the response regulator. Downstream of this transfer, phosphorylation of the aspartate causes long-range conformational changes throughout the receiver domain that shift its equilibrium from a monomer to dimer. Classically, the phosphorylation of the aspartate on the β3 strand has been described as causing a conformational switch in a β4 strand threonine, which is passed on to a β5 strand tyrosine (so-called "Y-T" coupling), which is in turn transmitted to the α4 and α5 helices that constitute the dimerization interface (Bachhawat and Stock, 2007; Bourret, 2010). Although "Y-T" coupling has been challenged (Campagne et al., 2016; Ouyang et al., 2019), it is clear that at least some response regulator receiver domains employ a different mechanism of signal transduction (Desai and Kenney, 2017). Despite the high degree of identity between AdeR and other receiver domains, we previously noted some striking differences. AdeR has a strong tendency to dimerize in the absence of phosphorylation, and a salt bridge was noted between the phosphorylation target D63 and K112 that is not observed in other receiver domains (Wen et al., 2017). In the present study, we observe that the D63-K112 interaction appears to be coupled to a folding-unfolding transition of helix α4, which is in turn coupled to structuring of the disordered N-terminal tail that lies across the dimeric interface. This novel conformational cascade presents multiple new potential mechanisms of regulation. The disordered N-terminal tail modifies the susceptibility of the entire protein to proteolytic degradation, constituting an important mechanism for its regulation, as shown in Figure S5. The N-terminal tail plays a role in maintenance of the cytoplasmic AdeR level, which can affect the AdeABC efflux pump. The mechanism is distinct from the well-characterized toxin-disordered N-terminal regulation in the toxin-antitoxin module, which is directly involved in the DNA binding of antitoxin (Garcia-Pino et al., 2016; Talavera et al., 2019). However, this also raises a possible mechanism of AdeR release after completing the recognition and activation of the AdeABC efflux pump: the AdeR dimer may be released by the N-terminal IDR and further enter into the degradation and homeostasis recycle pathway (Figure S5).

It is also known that AdeRS-mediated regulation of gene expression is susceptible to factors such as temperature, osmolarity, and small molecules like salicylate (Bazyleu and Kumar, 2014). With this present study, we have near-complete structures along the entire AdeRS axis, with the exception of the periplasmic loop and transmembrane helices, and yet it is still not apparent how AdeRS responds to such varied stimuli. We note that folding-unfolding transitions, such as was observed for the AdeR N-terminal tail and α4 helix, are sensitive to temperature and osmolarity. Thus, there are many sites along the AdeRS axis at which regulation by external stimuli can potentially take place.

Canonical sensor histidine kinases act as homodimers that can exhibit autophosphorylase, transphosphorylase, and dephosphorylase activities, but recent studies have defined noncanonical histidine kinases with hetero-oligomerization, as well as cross-phosphorylation between different histidine kinase domain (Stock et al., 2000; Willett and Crosson, 2017). The higher order oligomerization observed in some histidine kinases has been attributed to crystal packing, although it is thought to be important in atypical histidine kinases such as ExsG from *Rhizobium* NT-26 and cyanobacterial histidine kinase-2 (Ibrahim et al., 2018; Mechaly et al., 2014; Wojnowska et al., 2013). In the case of *Rhodobacter* spp RegB histidine kinase, tetramer formation inhibits autokinase activity (Swem et al., 2003). The hexameric active assembly of AdeS provides the first example of a prototypical HAMP-DHp-CA domain in which histidine kinase activity is activated by oligomerization (Figure S5).

Based on our integrative structural biology approach and homology modeling, we have constructed a theoretical model of the AdeS hexamer. This is possible by combining our X-ray structure of residues 138–357 with a

homology model for residues 84–137 based on known HAMP domain dimer structures and 1–83 transmembrane domain with sensory loop using the I-TASSER server (Yang and Zhang, 2015). It must also be noted that in the linker between HAMP and DHp domains, residues 138–148 were unstructured and not visible in the X-ray crystal structure. To assemble AdeS into a hexamer, these residues have to form a sharp bend that was not observed in CpxA, in which a continuous helix was observed in the corresponding residues (Mechaly et al., 2014). It should also be noted that formation of the hexameric AdeS requires a displacement of the CA domains. This would be necessary for them to access the target His149 residues anyways and would be consistent with the negative stain EM maps, particularly in the ATP-bound state. This may explain why inclusion of the HAMP domains and accompanying hexamer formation was necessary to stimulate catalytic activity.

In conclusion, we demonstrate novel mechanisms of regulation not previously seen in TCSs: activation of the histidine kinase AdeS through hexameric assembly and proteolytic degradation of an intrinsically disordered tail in its cognate response regulator, AdeR. These additional mechanisms further broaden our understanding of response regulation and the evolution of TCSs and may aid drug discovery efforts targeting TCSs.

Limitations of the study

The study presented a biophysical and structural study of the AdeRS TCS. However, the cryo-EM study of the full-length AdeS and the physiological significance of this regulatory mechanism remains to be investigated.

STAR★METHODS

Detailed methods are provided in the online version of this paper and include the following:

- KEY RESOURCES TABLE
- RESOURCE AVAILABILITY
  - Lead contact
  - Data and code availability
- METHODS DETAILS
- QUANTIFICATION AND STATISTICAL ANALYSIS
- ADDITIONAL RESOURCES

SUPPLEMENTAL INFORMATION

Supplemental information can be found online at https://doi.org/10.1016/j.isci.2021.102476.

ACKNOWLEDGMENTS

We thank the staff from the BL18U1/BL19U1 beamline and BL19U2 small angle X-ray scattering beamline for technical support during data collection at the National Center for Protein Sciences Shanghai (NCPSS) at Shanghai Synchrotron Radiation Facility. We also appreciate the Electron Microscopy Center of Lanzhou University, especially Dr. Deng Xia, for technical support. This work was supported by National Natural Science Foundation of China (NO.82072237, NO.31870132, NO.81741088 to Y. Wen, NO. 31600593 to Z.L.) and Shaanxi Province Natural Science Funding (NO. 2020-JQ084 to Y. Wen).

AUTHOR CONTRIBUTIONS

Y. Wen designed and conducted the project. Z.O., F.Z., Z.L., J.F., D.W., K.W., I.G., Y. Wu, P.M.H., J.S. carried out the experiments. Y. Wen, Z.O., Z.L., J.F., P.M.H., and J.S. analyzed the data. Y. Wen wrote the paper with contribution from all the authors.

DECLARATION OF INTERESTS

The authors declare no competing interest.

Received: November 6, 2020
Revised: March 15, 2021
Accepted: April 23, 2021
Published: May 21, 2021

REFERENCES

Bachhawat, P., and Stock, A.M. (2007). Crystal structures of the receiver domain of the response regulator PhoP from Escherichia coli in the absence and presence of the phosphoryl analog beryllofluoride. J. Bacteriol. *189*, 5987–5995. https://doi.org/10.1128/JB.00049-07.

Bachmair, A., Finley, D., and Varshavsky, A. (1986). In vivo half-life of a protein is a function of its amino-terminal residue. Science *234*, 179–186. https://doi.org/10.1126/science.3018930.

Bazyleu, A., and Kumar, A. (2014). Incubation temperature, osmolarity, and salicylate affect the expression of resistance-nodulation-division efflux pumps and outer membrane porins in Acinetobacter baumannii ATCC19606T. FEMS Microbiol. Lett. *357*, 136–143. https://doi.org/10.1111/1574-6968.12530.

Bourret, R.B. (2010). Receiver domain structure and function in response regulator proteins. Curr. Opin. Microbiol. *13*, 142–149. https://doi.org/10.1016/j.mib.2010.01.015.

Campagne, S., Dintner, S., Gottschlich, L., Thibault, M., Bortfeld-Miller, M., Kaczmarczyk, A., Francez-Charlot, A., Allain, F.H.T., and Vorholt, J.A. (2016). Role of the PFXFATG[G/Y] motif in the activation of SdrG, a response regulator involved in the alphaproteobacterial general stress response. Structure *24*, 1237–1247. https://doi.org/10.1016/j.str.2016.05.015.

Capra, E.J., and Laub, M.T. (2012). The evolution of two-component signal transduction systems. Annu. Rev. Microbiol. *66*, 325–347. https://doi.org/10.1016/j.pestbp.2011.02.012.

Craiu, A., Gaczynska, M., Akopian, T., Gramm, C.F., Fenteany, G., Goldberg, A.L., and Rock, K.L. (1997). Lactacystin and clasto-lactacystin β-lactone modify multiple proteasome β-subunits and inhibit intracellular protein degradation and major histocompatibility complex class I antigen presentation. J. Biol. Chem. *272*, 13437–13445. https://doi.org/10.1074/jbc.272.20.13437.

Desai, S.K., and Kenney, L.J. (2017). To ~P or Not to ~P? Non-canonical activation by two-component response regulators. Mol. Microbiol. *103*, 203–213. https://doi.org/10.1111/mmi.13532.

Garcia-Pino, A., De Gieter, S., Talavera, A., De Greve, H., Efremov, R.G., and Loris, R. (2016). An intrinsically disordered entropic switch determines allostery in Phd-Doc regulation. Nat. Chem. Biol. *12*, 490–496. https://doi.org/10.1038/nchembio.2078.

Gerson, S., Nowak, J., Zander, E., Ertel, J., Wen, Y., Krut, O., Seifert, H., and Higgins, P.G. (2018). Diversity of mutations in regulatory genes of resistance-nodulationcell division efflux pumps in association with tigecycline resistance in Acinetobacter baumannii. J. Antimicrob. Chemother. *73*, 1501–1508. https://doi.org/10.1093/jac/dky083.

Gotoh, Y., Eguchi, Y., Watanabe, T., Okamoto, S., Doi, A., and Utsumi, R. (2010). Two-component signal transduction as potential drug targets in pathogenic bacteria. Curr. Opin. Microbiol. *13*, 232–239. https://doi.org/10.1016/j.mib.2010.01.008.

Groisman, E.A. (2016). Feedback control of two-component regulatory systems. Annu. Rev. Microbiol. *70*, 103–124. https://doi.org/10.1146/annurev-micro-102215-095331.

Ibrahim, I.M., Wang, L., Puthiyaveetil, S., Krauß, N., Nield, J., and Allen, J.F. (2018). Oligomeric states in sodium ion-dependent regulation of cyanobacterial histidine kinase-2. Protoplasma *255*, 937–952. https://doi.org/10.1007/s00709-017-1196-7.

Kim, H.K., Kim, R.R., Oh, J.H., Cho, H., Varshavsky, A., and Hwang, C.S. (2014). The N-terminal methionine of cellular proteins as a degradation signal. Cell *156*, 158–169. https://doi.org/10.1016/j.cell.2013.11.031.

Marchand, I., Marchand, I., Damier-piolle, L., Damier-piolle, L., Courvalin, P., Courvalin, P., Lambert, T., and Lambert, T. (2004). Expression of the RND-type efflux pump AdeABC in acinetobacter baumannii is regulated by the AdeRS two-component system. Antimicrob. Agents Chemother. *48*, 3298–3304. https://doi.org/10.1128/AAC.48.9.3298.

Mechaly, A.E., Sassoon, N., Betton, J.M., and Alzari, P.M. (2014). Segmental helical motions and dynamical asymmetry modulate histidine kinase autophosphorylation. PLoS Biol. *12*, e1001776. https://doi.org/10.1371/journal.pbio.1001776.

Mechaly, A.E., Soto Diaz, S., Sassoon, N., Buschiazzo, A., Betton, J.-M., and Alzari, P.M. (2017). Structural coupling between autokinase and phosphotransferase reactions in a bacterial histidine kinase. Structure *25*, 939–944. https://doi.org/10.1016/j.str.2017.04.011.

Nowak, J., Schneiders, T., Seifert, H., and Higgins, P.G. (2016). The Asp20-to-Asn substitution in the response regulator AdeR leads to enhanced efflux activity of AdeB in Acinetobacter baumannii. Antimicrob. Agents Chemother. *60*, 1085–1090. https://doi.org/10.1128/AAC.02413-15.

Ouyang, Z., Zheng, F., Chew, J.Y., Pei, Y., Zhou, J., Wen, K., Han, M., Lemieux, M.J., Hwang, P.M., and Wen, Y. (2019). Deciphering the activation and recognition mechanisms of Staphylococcus aureus response regulator ArlR. Nucleic Acids Res. *47*, 11418–11429. https://doi.org/10.1093/nar/gkz891.

Stock, A.M., Robinson, V.L., and Goudreau, P.N. (2000). Two-component signal transduction. Annu. Rev. Biochem. *69*, 183–215. https://doi.org/10.1146/annurev.biochem.69.1.183.

Swem, L.R., Kraft, B.J., Swem, D.L., Setterdahl, A.T., Masuda, S., Knaff, D.B., Zaleski, J.M., and Bauer, C.E. (2003). Signal transduction by the global regulator RegB is mediated by a redox-active cysteine. EMBO J. *22*, 4699–4708. https://doi.org/10.1093/emboj/cdg461.

Talavera, A., Tamman, H., Ainelo, A., Konijnenberg, A., Hadži, S., Sobott, F., Garcia-Pino, A., Hõrak, R., and Loris, R. (2019). A dual role in regulation and toxicity for the disordered N-terminus of the toxin GraT. Nat. Commun. *10*, 1–13. https://doi.org/10.1038/s41467-019-08865-z.

Varshavsky, A. (2011). The N-end rule pathway and regulation by proteolysis. Protein Sci. *20*, 1298–1345. https://doi.org/10.1002/pro.666.

Wen, Y., Ouyang, Z., Yu, Y., Zhou, X., Pei, Y., Devreese, B., Higgins, P.G., and Zheng, F. (2017). Mechanistic insight into how multidrug resistant Acinetobacter baumannii response regulator AdeR recognizes an intercistronic region. Nucleic Acids Res. *45*, 9773–9787. https://doi.org/10.1093/nar/gkx624.

Willett, J.W., and Crosson, S. (2017). Atypical modes of bacterial histidine kinase signaling. Mol. Microbiol. *103*, 197–202. https://doi.org/10.1111/mmi.13525.

Wojnowska, M., Yan, J., Sivalingam, G.N., Cryar, A., Gor, J., Thalassinos, K., and Djordjevic, S. (2013). Autophosphorylation activity of a soluble hexameric histidine kinase correlates with the shift in protein conformational equilibrium. Chem. Biol. *20*, 1411–1420. https://doi.org/10.1016/j.chembiol.2013.09.008.

Yang, J., and Zhang, Y. (2015). I-TASSER server: new development for protein structure and function predictions. Nucleic Acids Res. *43*, W174–W181. https://doi.org/10.1093/nar/gkv342.

Yoon, E.J., Courvalin, P., and Grillot-Courvalin, C. (2013). RND-type efflux pumps in multidrug-resistant clinical isolates of Acinetobacter baumannii: major role for AdeABC overexpression and aders mutations. Antimicrob. Agents Chemother. *57*, 2989–2995. https://doi.org/10.1128/AAC.02556-12.

Yoon, E.J., Chabane, Y.N., Goussard, S., Snesrud, E., Courvalin, P., Dé, E., and Grillot-Courvalin, C. (2015). Contribution of resistance-nodulation-cell division efflux systems to antibiotic resistance and biofilm formation in Acinetobacter baumannii. mBio *6*, 1–13. https://doi.org/10.1128/mBio.00309-15.

Ōmura, S., and Crump, A. (2019). Lactacystin: first-in-class proteasome inhibitor still excelling and an exemplar for future antibiotic research. J. Antibiot. (Tokyo) *72*, 189–201. https://doi.org/10.1038/s41429-019-0141-8.

STAR★METHODS

KEY RESOURCES TABLE

REAGENT or RESOURCE	SOURCE	IDENTIFIER
Antibodies		
6*His, His-Tag Monoclonal antibody	Proteintech	Cat#: 66005-1-Ig
Goat Anti-Mouse IgG second antibody	Sigma-Aldrich	Cat#: 401215
Bacterial and virus strains		
E. coli BL21 Star™ (DE3)	Thermofisher	Cat#: C601003
E. coli DH5α	Thermofisher	Cat#: EC0112
Acinetobacter baumannii	ATCC	ATCC19606
Chemicals, peptides, and recombinant proteins		
Clasto-Lactacystin β-lactone	Cayman chemical	Cat#: 70988
Critical commercial assays		
Transcriptor First Strand cDNA Synthesis Kit	Roche	Cat#: 04379012001
FastStart Essenti al DNA Green Master	Roche	Cat#: 04 673 484 001
Clarity™ Western ECL Substrate	BIO-RED	Cat #: 1705060
ADP-Glo™ Kinase Assay kit	Promega	Cat #:V6930
Data and Code availability		
Structure factor of AdeR	PDB	7CCI
Structure factor of AdeS	PDB	7CCH
SAXS data of AdeS DHp-CA	SASBDB	SASDK48
SAXS data of AdeS Cytoplasmic domain	SASBDB	SASDK58
EM data of AdeS apo	EMDB	EMD-30929
EM data of AdeS ATP bound	EMDB	EMD-30930
Oligonucleotides		
AdeS-full-F: CATGCCATGGGCCATCATCATCAT CATCACAAAAGTAAGTTAGGAATT AGTAAGCAAC	This paper	N/A
AdeS-full-R: CCGCTCGAGTTAGTTATTCATAGA AATTTTTATGGTG	This paper	N/A
AdeS-Cytoplasmic-F: CATGCCATGGGCCATCATCATCAT CATCACAAGCGTTTTATTGTGCCA A	This paper	N/A
AdeS-DHp-CA-F: CATGCCATGGGCCATCATCATCAT CATCACGCCATCGCACATGAGTTA	This paper	N/A
AdeS-HAMP+DHp-R: CCGCTCGAGTTATTGCTGGTTCTCT ACTAAGCTTAAAG	This paper	N/A
A.b-16sRNA forward: CAGCTCGTGTCGTGAGATGT	This paper	N/A

(*Continued on next page*)

Continued

REAGENT or RESOURCE	SOURCE	IDENTIFIER
A.b-16sRNA reverse: CGTAAGGGCCATGATGACTT	This paper	N/A
qPCR-AdeB-F: GGCACTTTGTGCCACGATTT	This paper	N/A
qPCR-AdeB-R: TCTTGGCTGCCATTGCCATA	This paper	N/A

RESOURCE AVAILABILITY

Lead contact

Further requests and materials should be directed to and will be fulfilled by the lead contact Dr. Yurong Wen (Yurong.Wen@xjtu.edu.cn).

Data and code availability

Atomic coordinates and structure factors for the AdeR and AdeS have been deposited in the Protein Data Bank with accession codes 7CCI and 7CCH, respectively. The SAXS data and analysis for the AdeS DHp-CA and cytoplasmic domain has been deposited in the SASBDB under the accession codes of SASDK48 and SASDK58. The EM map of the AdeS apo and ATP-bound form has been submitted to the EMDB with the accession codes EMD-30929 and EMD-30930, respectively.

METHODS DETAILS

All methods details can be found in the accompanying Star Methods Supplemental file.

QUANTIFICATION AND STATISTICAL ANALYSIS

Statistical analysis was done with an unpaired t-test.

ADDITIONAL RESOURCES

Additional resources can be found in the supplemental key resource table.